Cell

Article

# Unraveling the Biology of a Fungal Meningitis Pathogen Using Chemical Genetics

Jessica C.S. Brown,[1,6] Justin Nelson,[2] Benjamin VanderSluis,[2] Raamesh Deshpande,[2] Arielle Butts,[3] Sarah Kagan,[4] Itzhack Polacheck,[4] Damian J. Krysan,[3,5] Chad L. Myers,[2,*] and Hiten D. Madhani[1,*]

[1]Department of Biochemistry and Biophysics, University of California, San Francisco, San Francisco, CA 94158, USA

[2]Department of Computer Science and Engineering, University of Minnesota, Minneapolis, MN 55455, USA

[3]Department of Chemistry, University of Rochester Medical Center, Rochester, NY 14643, USA

[4]Department of Clinical Microbiology and Infection Diseases, Hadassah-Hebrew University Medical Center, Jerusalem 91120, Israel

[5]Departments of Pediatrics and Microbiology/Immunology, University of Rochester School of Medicine and Dentistry, Rochester, NY 14643, USA

[6]Present address: Department of Pathology, Division of Microbiology and Immunology, University of Utah School of Medicine, Salt Lake City, UT 84112, USA

*Correspondence: cmyers@cs.umn.edu (C.L.M.), hitenmadhani@gmail.com (H.D.M.)

http://dx.doi.org/10.1016/j.cell.2014.10.044

## SUMMARY

The fungal meningitis pathogen *Cryptococcus neoformans* is a central driver of mortality in HIV/AIDS. We report a genome-scale chemical genetic data map for this pathogen that quantifies the impact of 439 small-molecule challenges on 1,448 gene knockouts. We identified chemical phenotypes for 83% of mutants screened and at least one genetic response for each compound. *C. neoformans* chemical-genetic responses are largely distinct from orthologous published profiles of *Saccharomyces cerevisiae*, demonstrating the importance of pathogen-centered studies. We used the chemical-genetic matrix to predict novel pathogenicity genes, infer compound mode of action, and to develop an algorithm, O2M, that predicts antifungal synergies. These predictions were experimentally validated, thereby identifying virulence genes, a molecule that triggers G2/M arrest and inhibits the Cdc25 phosphatase, and many compounds that synergize with the antifungal drug fluconazole. Our work establishes a chemical-genetic foundation for approaching an infection responsible for greater than one-third of AIDS-related deaths.

## INTRODUCTION

Invasive fungal infections are notoriously difficult to diagnose and treat, resulting in high mortality rates, even with state-of-the art treatments. The three most common pathogenic agents are *Cryptococcus neoformans, Candida albicans*, and *Aspergillus fumigatus* (Mandell et al., 2010). These organisms are opportunistic fungi that prey on individuals with varying degrees of immune deficiency. Susceptible patient populations include premature infants, diabetics, individuals with liver disease, chemotherapy patients, organ transplant recipients, and those infected with HIV (Mandell et al., 2010). Compounding the clinical challenge is the slow pace of antifungal drug development: only a single new class of drugs (the echinocandins) has been approved for use in the United States in the last 30 years (Butts and Krysan, 2012; Mandell et al., 2010; Roemer et al., 2011).

Fungal infections are estimated to cause 50% of deaths related to AIDS and have been termed a "neglected epidemic" (Armstrong-James et al., 2014). The fungus chiefly responsible for deaths in this population is *C. neoformans* (Armstrong-James et al., 2014). *C. neoformans* is an encapsulated basidiomycetous haploid yeast distantly related to *Saccharomyces cerevisiae* and *Schizosaccharomyces pombe*. A 2009 CDC study estimated that ~1 million infections and ~600,000 deaths annually are caused by *C. neoformans*, exceeding the estimated worldwide death toll from breast cancer (Lozano et al., 2012; Park et al., 2009). *C. neoformans* is widespread in the environment and exposure occurs through inhalation of desiccated yeast or spores (Heitman et al., 2011). In immunocompromised patients, *C. neoformans* replicates and disseminates, causing meningoencephalitis that is lethal without treatment (Heitman et al., 2011). Induction therapy involves flucytosine and intravenous infusions of amphotericin B (Loyse et al., 2013). Both drugs are highly toxic, difficult to administer, and neither is readily available in the areas with the highest rates of disease. The current recommendation for Cryptococcosis treatment is at least a year of therapy, which is difficult to accomplish in resource-limited settings (WHO, 2011). Thus, as is the case with infections caused by other fungal pathogens, effective treatment of cryptococcal infections is limited by the efficacy, toxicity, and availability of current pharmaceuticals.

We implemented chemogenomic profiling to approach the challenges of therapeutic development in *C. neoformans*. This method involves the systematic measurement of the impact of compounds on the growth of defined null mutants to produce a chemical-genetic map. Such a map represents a quantitative description composed of numerical scores indicative of the growth behavior of each knockout mutant under each chemical condition. Cluster analysis of the growth scores for large

numbers of mutants under many chemical conditions can reveal genes that function in the same pathway and even those whose products are part of the same protein complex (Collins et al., 2007; Parsons et al., 2004; Parsons et al., 2006). In addition, the identity of genes whose mutation produce resistance or sensitivity is useful for uncovering compound mode of action (MOA) (Hillenmeyer et al., 2008; Jiang et al., 2008; Nichols et al., 2011; Parsons et al., 2006; Xu et al., 2007; Xu et al., 2009). Large-scale studies have been restricted to model organisms for which gene deletion collections have been constructed, namely *S. cerevisiae*, *S. pombe*, and *Escherichia coli* K12 (Hillenmeyer et al., 2008; Nichols et al., 2011; Parsons et al., 2006). However, as none of these are pathogens, the extent to which the resulting insights translate to pathogenic organisms is unknown. A variation on chemogenomic profiling, chemically-induced haploinsufficiency, was first developed using a diploid heterozygote gene deletion library *S. cerevisiae* to identify compound MOA. This method, which identifies genes that impact compound sensitivity based on a two-fold gene dosage change, is suited for diploid organisms and has been used in the pathogen *C. albicans* (Jiang et al., 2008; Xu et al., 2007; Xu et al., 2009).

We report here the generation of a large-scale chemogenomic map for *C. neoformans* using defined, commonly available knockout mutants, assessments of data quality, and extensive experimental verification. Comparisons of the *C. neoformans* profile with two large-scale published profiles from *S. cerevisiae* revealed that for most types of compounds, the chemical-genetic interactions are distinct even among orthologous genes, emphasizing the importance of pathogen-focused investigation. We used nearest-neighbor analysis to predict new genes involved in polysaccharide capsule formation and infectivity, which we validated through experiment. We also utilized genetic responses to predict the G2/M phase of the cell cycle and the Cdc25 phosphatase as targets of a thiazolidone-2,4-dione derivative, which we confirmed in vivo and in vitro. Finally, because of the unmet need for improved antifungal drug efficacy, we developed a new algorithm, O2M, to predict new compound synergies based on the profiles of pairs known to be synergistic. Experimental tests demonstrate that the method performs vastly better than random expectation, thereby enabling the identification of synergistic compound combinations. Our studies establish a chemical-genetic foundation to approach the biology and treatments of *C. neoformans* infections, which are responsible for more than one-third of HIV/AIDS deaths worldwide.

## RESULTS

### A Chemical-Genetic Map of *C. neoformans*

We assembled 1,448 *C. neoformans* gene deletion strains (Chun et al., 2011; Liu et al., 2008) (Table S1 available online), corresponding to a substantial fraction of 6,967 predicted *C. neoformans* genes (Janbon et al., 2014), and a collection of compounds for screening (Table 1). Compounds were selected based on cost and literature evidence that they could inhibit the growth of fungi. Where feasible, compounds were chosen that are known to target specific biological processes. For each small molecule, we determined an approximate minimum inhibitory concentration (MIC) in agar, then measured growth of the knockout collection on each small molecule at 50%, 25%, and 12.5% MIC using high density agar plate colony arrays and a robotic replicator. We then measured the size of each colony using flatbed scanning and colony measurement software (Dittmar et al., 2010). We performed a minimum of four replicate colony measurements for each mutant-condition pair. Plate-based assays are subject to known nonbiological effects, such as spatial patterns. To mitigate these errors, a series of corrective measures were implemented using approaches described previously, including manual filtration of noisy data, spatial effect normalization and machine learning-based batch correction (Baryshnikova et al., 2010). In addition, the data for each deletion mutant and compound was centered and normalized. Each mutant-small molecule combination was assigned a score with positive scores representing relative resistance and negative scores representing compound sensitivity (Table S2). A global summary of the processed data organized by hierarchical clustering is shown in Figure 1A.

The importance and validity of the computational corrections is shown in Figures 1B and S1. We estimated how reproducible the chemical-genetic profiles were by calculating the correlation scores for data obtained for different concentrations of the same small molecule (purple). This measures the degree of overlap between the overall chemical-genetic profiles, which are themselves each composed of a score for each mutant-small molecule combination. We found significant correlation ($p = 2.67 \times 10^{-176}$) between data obtained for different concentrations of the same small molecule compared to those between profiles generated by data set randomization, suggesting significant reproducibility. Moreover, correlation scores between chemical-genetic profiles of different concentrations of different compounds (gray) are centered at approximately 0 (Figure 1B). This difference in correlation scores is apparent even when comparing experiments performed on the same day, when spurious batch signal can contribute to false positives (Baryshnikova et al., 2010). Our batch-correction algorithms resulted in same-batch screening data with strong positive correlation scores for the same compounds but correlation scores close to zero for different compounds (Figure S1), demonstrating successful removal of spurious signal (Baryshnikova et al., 2010). We compared chemical-genetic profiles between compounds in the azole family (Figure 1C). Despite the fact that the azoles tested include those of diverse uses, from agricultural pesticides to FDA-approved drugs (Table 1), many exhibit a significant profile correlation ($p = 2.82 \times 10^{-6}$), further indicating significant signal in the data. As a final assessment, we performed hypergeometric testing across all compounds to determine whether the same sensitive gene knockouts (defined by $Z < -2.5$) are identified at different concentrations of the same compounds. Using a Bonferonni-corrected p value cutoff, nearly all compounds display significant overlap of responsive genes at different concentrations (Figure 1D).

We assigned at least one phenotype (sensitivity or resistance to a compound) to 1,198 of 1,448 mutants (Figure 1E, Tables S2, S3, and S4). Of these, 855 exhibit one to ten phenotypes, while remaining 343 displayed from 11 to 146 phenotypes. Gene

**Table 1. Small Molecules and Targets**

| Inhibitor (Activator) | Highest Screening Conc. | Process/Enzyme | Category | Pubchem ID | FDA Approval? |
|---|---|---|---|---|---|
| 1-10 phenanthroline hydrochloride monohydrate | 2 uM | broad/transition metal complexes | broad spectrum | 2723715 | no |
| 2-aminobenzothiazole | 30 uM | cytoskeleton function/ kinesin Kip1 | cell structure | 8706 | no |
| 2-hydroxyethylhydrazine | 0.156% | lipid synthesis/phospholipid methylation | lipid biosynthesis | 8017 | no |
| 3-aminotriazole | 6.25 mM | histidine synthesis/IMP dehydratase | metabolism | 1639 | no |
| 4-hydroxytamoxifen | 1.56 uM | estrogen receptor (mammals) | signaling | 449459 | yes |
| 5-fluorocytosine | 2.5 ug/ml | DNA/RNA biosynthesis | DNA homeostasis/ protein synthesis | 3366 | yes |
| 5-methyltryptophan | 8 mM | tryptophan synthesis | metabolism | 150990 | no |
| Abietic acid | 1 mM | lipid synthesis/lipoxygenase | lipid biosynthesis | 10569 | no |
| Acifluorfen methyl | 156.25 ng/ml | porphyrin synthesis/ protoporphyrinogen oxidase | metabolism | 91642 | no |
| (Aconitine) | 200 ug/ml | membrane potential/$Na^+$ channels (mammals) | membrane polarization | 245005 | no |
| Aflatoxin B1 | 100 ug/ml | DNA damaging agent | DNA homeostasis | 14403 | no |
| Agelasine D | 5 ug/ml | membrane potential/$Na^+$/ K+-ATPase (mammals) | membrane polarization | 46231918 | no |
| Alamethicin/U-22324 | 60 uM | membrane integrity/forms a voltage-depended ion channel | membrane polarization | 16132042 | no |
| Alexidine dihydrochloride | 125 ug/ml | antimicrobial/mitochondria | mitochondria | 102678 | yes |
| Allantoin | 100 ug/ml | nitrogen-rich compound | metabolism | 204 | topical |
| Alternariol | 2.5 ug/ml | cholinesterase inhibitor/sodium channel activator and DNA supercoiling/topoisomerase I | broad spectrum | 5359485 | no |
| Alumininum sulfate | 1.5625 mM | unknown | unknown | 24850 | no |
| (Amantadine hydrochloride) | 1.25 mM | neurotransmitter release/ glutamate receptor | signaling | 64150 | yes |
| Amiodarone | 60 ug/ml | membrane potential/$Na^+$/ K+-ATPase (mammals) | membrane polarization | 2157 | yes |
| (Ammonium persulfate) | 50 mM | reactive oxygen species | apoptosis/stress response/ damage response | 62648 | no |
| Amphotericin B | 1 ug/ml | lipid biosynthesis/ergosterol | membrane integrity | 5280965 | yes |
| Andrastin A | 4 ug/ml | protein modification/ farnesyltransferase | protein trafficking | 6712564 | no |
| Anisomycin | 50 uM | translation/peptidyl transferase | gene expression | 253602 | no |
| Antimycin | 100 ug/ml | respiration/cytochrome B | metabolism | 14957 | no |
| Apicidin | 312.5 ng/ml | chromatin regulation/HDACs | gene expression | 6918328 | no |
| Artemisinin | 312.5 mM | iron metabolism/hematin detoxification | metabolism | 68827 | yes |
| Ascomycin | 3.125 uM | signaling/calcineurin | signaling | 6437370 | yes |
| Azide | 62.5 uM | respiration/cytochrome C oxidase | metabolism | 33558 | no |
| Barium chloride | 16 mM | metal homeostasis/diverse | broad spectrum/unknown | 25204 | no |
| Bafilomycin | 4 ug/ml | autophagy/vacuolar-type $H^+$-ATPase | protein turnover | 6436223 | no |
| Bathocuproine disulphonic acid (BCS) | 3 mM | copper acquisition | metabolism | 16211287 | no |

(*Continued on next page*)

**Table 1.** *Continued*

| Inhibitor (Activator) | Highest Screening Conc. | Process/Enzyme | Category | Pubchem ID | FDA Approval? |
|---|---|---|---|---|---|
| Bathophenanthroline disulfonate (BPS) | 300 uM | iron acquistion/Fet3-Ftr1 | metabolism | 65368 | no |
| Benomyl | 100 ug/ml | cytoskeleton function/tubulin | cell structure | 28780 | no |
| (Betulinic acid) | 64 ug/ml | protein degradation/proteasome | protein turnover | 64971 | no |
| Bifonazole | 50 ug/ml | lipid biosynthesis/HMG-CoA and ergosterol biosynthesis | membrane integrity | 2378 | no |
| Brefeldin A | 40 ug/ml | ER-Golgi Transport/ARF GEF | secretion | 5287620 | no |
| Calcium chloride | 16 mM | metal homeostasis/diverse | broad spectrum | 5284359 | no |
| Caffeine | 2.5 mM | DNA damage checkpoint/ATM | DNA homeostasis | 2519 | no |
| Calcium ionophore A23187 | 2.5 ug/ml | membrane integrity/peptide that acts as ionophore | membrane integrity | 40486 | no |
| Calcofluor white | 500 ug/ml | cell wall synthesis/chitin and cellulose | cell wall | 6108780 | no |
| Camptothecin | 500 ug/ml | DNA supercoiling/topoisomerase I | DNA homeostasis | 24360 | analog |
| Castanospermine | 2.4 mM | protein modification/glycosidation | protein modification | 54445 | derivative |
| Cadmium chloride | 1 mM | metal homeostasis/diverse | broad spectrum/unknown | 24947 | no |
| Cerulenin | 312.5 ng/ml | fatty acid synthesis/beta-ketoacyl-acyl carrier protein synthase | lipid biosynthesis | 5282054 | no |
| Cesium chloride | 128 mM | metal homeostasis/diverse | broad spectrum/unknown | 24293 | no |
| Chlorpromazine hydrochloride | 1.5625 uM | phenothiazine antipsychotic drug (mammals)/dopamine, seratonin, and other neuroreceptors | signaling | 6240 | yes |
| Chromium (III) chloride | 8 mM | metal homeostasis/diverse | broad spectrum | 16211596 | no |
| Ciclopirox olamine | 750 ng/ml | iron acquisition and other | metabolism | 38911 | yes |
| Cisplatin | 100 ug/ml | DNA synthesis | DNA homeostasis | 157432 | yes |
| Climbazole | 0.03125% | lipid biosynthesis/ergosterol biosynthesis and respiration/ cytochrome P450 | broad spectrum | 37907 | topical |
| Clotrimazole | 500 nM | lipid biosynthesis/ergosterol biosynthesis | membrane integrity | 2812 | yes |
| Colistin | 1 mg/ml | membrane integrity | membrane integrity | 5311054 | yes |
| Congo red | 0.0625% | cell wall synthesis/chitin, cellulose, and glucan | cell wall | 11313 | no |
| Coniine | 0.15625% | neurosignaling (mammals)/ nicotinic receptor | signaling | 441072 | no |
| (Crystal violet) | 0.0012500% | oxidative stress inducer | stress response | 11057 | topical |
| CuCl2 | 8 mM | copper homeostasis/diverse | metabolism | 24014 | no |
| Cycloheximide | 1.875 ug/ml | translation/ribosome | gene expression | 6197 | no |
| Cyclopiazonic acid | 15.625 uM | ion transport and cell polarization (mammals)/$Ca^{2+}$- ATPase | metabolism | 54682463 | no |
| Cyclosporin | 75 ug/ml | signaling/calcineurin | signaling | 5284373 | yes |
| Cyproconazole | 1.5625 ug/ml | lipid biosynthesis/ergosterol biosynthesis | membrane integrity | 86132 | no |
| Cyprodinil | 10 ug/ml | methionine biosynthesis | metabolism | 86367 | no |
| Daphnetin | 100 uM | signaling/PKA, PKC, EGR receptor, others | signaling | 5280569 | no |
| Desipramine hydrochloride | 250 uM | neurosignaling (mammals)/ norepinephrine transporter | signaling | 65327 | yes |

(*Continued on next page*)

**Table 1.** *Continued*

| Inhibitor (Activator) | Highest Screening Conc. | Process/Enzyme | Category | Pubchem ID | FDA Approval? |
|---|---|---|---|---|---|
| Dyclonine hydrochloride | 3.125 uM | lipid biosynthesis/ergosterol biosynthesis | membrane integrity | 68304 | yes |
| Emetine dihydrochloride hydrate | 5 mM | translation/ribosome | gene expression | 3068143 | yes |
| Emodin | 62.5 uM | signaling/CK2, others | signaling | 3220 | yes |
| Erlotinib | 50 ug/ml | signaling (mammals)/EGFR tyrosine kinase | signaling | 176870 | yes |
| FeCl3 | 32 mM | iron acquisition, metal homeostasis | metabolism | 24380 | no |
| Fenoxanil | 80 ug/ml | melanin biosynthesis | metabolism | 11262655 | no |
| Fenpropimorph | 2.5 ug/ml | sterol synthesis | lipid biosynthesis | 93365 | no |
| FK506 | 312.5 ng/ml | signaling/calcineurin | signaling | 445643 | yes |
| Fluconazole | 10 ug/ml | lipid biosynthesis/ergosterol biosynthesis | membrane integrity | 3365 | yes |
| Fluspirilene | 25 uM | antipsychotic drug, mechanism of action unknown | unknown | 3396 | yes |
| Gallium (III) nitrate | 25 mM | metal homeostasis/diverse | broad spectrum | 57352728 | no |
| Geldanamycin | 2 uM | protein folding/Hsp90 | protein folding | 5288382 | trials |
| (H2O2) | 6 mM | reactive oxygen species | apoptosis/ stress response/damage response | 784 | topical |
| Haloperidol | 125 uM | phenothiazine antipsychotic drug (mammals)/dopamine, seratonin, and other neuroreceptors | signaling | 3559 | yes |
| Harmine hydrochloride | 1 mM | cell differentiation (mammals)/ PPARgamma | signaling | 5359389 | yes |
| Hydroxyurea | 12.5 mM | DNA replication/replication fork progression | DNA homeostasis | 3657 | yes |
| Hygromycin | 37.5 ug/ml | translation/ribosome | gene expression | 35766 | no |
| Imazalil | 25 ug/ml | lipid biosynthesis/ergosterol synthesis | membrane integrity | 37175 | no |
| Iodoacetate | 500 uM | protein degradation/cysteine peptidases | protein turnover | 5240 | no |
| Itraconazole | 1.5625 ug/ml | lipid biosynthesis/ergosterol synthesis | membrane integrity | 55283 | yes |
| K252a | 10 ug/ml | signaling/variety of kinases | signaling | 127357 | trials |
| Latrunculin | 25 uM | cytoskeleton function/actin | cell structure | 445420 | no |
| Lead (II) nitrate | 64 mM | metal homeostasis/diverse | broad spectrum | 24924 | no |
| Leptomycin | 1.25 ug/ml | nucleocytoplasmic transport/ Crm1 | gene expression | 6917907 | no |
| LiCl | 37.5 mM | metal homeostasis/diverse | broad spectrum/ unknown | 433294 | no |
| Lovastatin | 37.5 ug/ml | sterol synthesis/HMG CoA reductase | metabolism | 53232 | yes |
| LY 294002 | 375 uM | signaling/PI3K | signaling | 3973 | no |
| Magnesium chloride | 150 mM | metal homeostasis/diverse | broad spectrum | 21225507 | no |
| Malachite green | 3.125 ug/ml | antimicrobial/unknown | antimicrobial | 11294 | no |
| Manganese sulfate | 128 mM | metal homeostasis/diverse | metabolism | 177577 | no |
| Mastoparan | 5 uM | signaling/G-proteins | signaling | 5464497 | no |
| (Menadione) | 150 uM | vitamin K3/reactive oxygen species | diverse | 4055 | yes |

(*Continued on next page*)

**Table 1.** *Continued*

| Inhibitor (Activator) | Highest Screening Conc. | Process/Enzyme | Category | Pubchem ID | FDA Approval? |
|---|---|---|---|---|---|
| Menthol | 1 mM | voltage-dependent ion channels (mammals)/sodium channel | signaling | 16666 | yes |
| Methotrexate | 2.5 uM | folate synthesis/DHFR | metabolism | 126941 | yes |
| Methyl methanesulfonate (MMS) | 0.0165% | DNA replication/replication fork progression | DNA homeostasis | 4156 | no |
| Methylbenzethonium chloride (MBT) | 0.25% | antimicrobial | antimicrobial | 5702238 | topical |
| MG132 | 12.5 uM | protein degradation/proteasome | protein turnover | 462382 | no |
| Miconazole | 6.25 ug/ml | lipid biosynthesis/ergosterol synthesis | membrane integrity | 4189 | yes |
| Mitomycin C | 12 uM | DNA damaging agent | DNA homeostasis | 5746 | yes |
| Myclobutanil | 2 ug/ml | lipid biosynthesis/ergosterol synthesis | membrane integrity | 6336 | no |
| Mycophenolic acid | 2.5 ug/ml | GMP synthesis/IMP dehydrogenase | metabolism | 446541 | yes |
| Myriocin | 12.5 ug/ml | sphingolipid synthesis | metabolism | 6438394 | analog |
| NA8 | | unknown | unknown | | no |
| (NaCl) | 37.5 mM | osmotic regulation/HOG pathway | stress response | 5234 | yes |
| (NaNO2) | 150 uM | reactive nitrogen species | stress response | 23668193 | no |
| Neomycin sulfate | 2.4 mM | protein synthesis/ribosome | gene expression | 8378 | yes |
| Nicotinamide | 25 uM | chromatin regulation/sirtuins | gene expression | 936 | yes |
| Nigericin | 100 ug/ml | membrane integrity/ion gradient | membrane polarization | 34230 | no |
| Nikkomycin | 5 ug/ml | chitin synthesis | cell wall | 72479 | trials |
| NiSO4 | 1 mM | antifungal/diverse | antifungal | 5284429 | no |
| Nocodazole | 30 uM | cytoskeleton function/tubulin | cell structure | 4122 | no |
| Ophiobolin A | 62.5 ng/ml | signaling/calmodulin | signaling | 5281387 | no |
| Parthenolide | 150 uM | immune and inflammatory response/NF-kB | signaling | 6473881 | no |
| Pentamidine isethionate | 500 uM | antimicrobial/mitochondrial function | antimicrobial | 8813 | yes |
| pH | 8.0, 8.5, 9.0 | pH homeostasis | diverse | | no |
| Phenylarsine oxide | 2.5 uM | broad/XCXXCX protein phosphatases | broad spectrum | 4778 | no |
| Picoxystrobin | 6.25 ug/ml | quinone outside inhibitor class/fungal cytochrome bcl | mitochondria | 11285653 | no |
| (Plumbagin) | 2.8 uM | reactive oxygen species | stress response | 10205 | no |
| PMSF | 10 mM | vacuolar proteolysis/ proteinase B | signaling | 4784 | no |
| Polyoxin B | 200 ug/ml | chitin synthesis | cell wall | 3084093 | no |
| Povidone iodine | 2% | antimicrobial | antimicrobial | 410087 | topical |
| Prussian blue | 75 mM | monocation chelator | metabolism | 16211064 | yes |
| Quinic acid | 2 mM | antimicrobial | antimicrobial | 6508 | no |
| Rapamycin | 0.125 uM | signaling/TOR kinases | signaling | 5284616 | yes |
| Rubidium chloride | 150 mM | potassium metabolism/ competitor | metabolism | 62683 | no |
| Rifamycin SV monosodium salt | 200 ug/ml | RNA synthesis/RNA polymerase | gene expression | 6324616 | yes |
| S10 | | unknown | unknown | | no |
| S8 | | unknown | unknown | | no |

(*Continued on next page*)

**Table 1.** *Continued*

| Inhibitor (Activator) | Highest Screening Conc. | Process/Enzyme | Category | Pubchem ID | FDA Approval? |
|---|---|---|---|---|---|
| S-aminoethyl-L-cysteine (thialysine) | 10 uM | amino acid metabolism/lysine analog | metabolism | 20048 | no |
| SDS | 0.0015625% | cell membrane integrity | membrane integrity | 3423265 | no |
| Selumetinib | 150 ug/ml | signaling/MAPK (ERK) | signaling | 10127622 | trials |
| Sertraline | 15 ug/ml | neurosignaling (mammals)/ seratonin reuptake | neurosignaling | 68617 | yes |
| Sodium azide | 62.5 uM | respiration/cytochrome oxidase | mitochondria | 33557 | no |
| Sodium borate | 10 mM | antimicrobial/diverse | antimicrobial | 21749317 | no |
| Sodium hydrosulfite | 6.25 mM | antimicrobial, counteracts some antimicrobials | antimicrobial | 24489 | no |
| Sodium iodide | 75 mM | antimicrobial | antimicrobial | 5238 | yes |
| Sodium metavanadate | 10 mM | signaling/protein phosphotyrosine phosphatases | signaling | 4148882 | no |
| (Sodium molybdate) | 64 mM | respiration/oxygen uptake | diverse | 61424 | no |
| Sodium selenite | 4 mM | respiration/oxygen uptake | diverse | 16210997 | yes |
| Sodium sulfite | 100 mM | ATP synthesis and accumulation/ unknown | metabolism | 24437 | no |
| Sodium tungstate | 64 mM | metal homeostasis/diverse | broad spectrum/unknown | 150191 | no |
| Sorafenib | 100 uM | signaling/VEGF tyrosine kinase | signaling | 216239 | yes |
| Staurosporine | 3 uM | signaling/PKC1 | signaling | 5279 | yes |
| (STF-62247) | 400 uM | autophagy | protein turnover | 704473 | trials |
| Sulfometuron methyl | 100 ug/ml | branch chain amino acid synthesis/acetolactate synthase | metabolism | 52997 | no |
| Suloctidil | 400 uM | $Ca^{2+}$ homeostasis in blood vessels (mammals)/putative $Ca^{2+}$ channel blocker | vascular system/ metabolism | 5354 | formerly |
| Tamoxifen citrate | 10 uM | estrogen signaling (mammals)/ estrogen receptor, mixed agonist/antagonist | signaling | 2733525 | yes |
| Taurolidine | 0.01% | antimicrobial/lipopolysaccharide detection and signaling | host defense | 29566 | yes |
| Tautomycin | 250 nM | signaling/PP2A | signaling | 3034761 | no |
| Tellurite | 0.1% | sulfate assimilation | metabolism | 115037 | no |
| Terbinafine | 75 uM | sterol synthesis/squalene epoxidase | metabolism | 1549008 | yes |
| Thiabendazole | 200 ug/ml | respiration/NADH oxidase | mitochondria | 5430 | yes |
| Thonzonium bromide | 25 uM | antimicrobial, pH homeostasis/ V-ATPase | broad spectrum | 11102 | yes |
| Tomatine | 5 ug/ml | glycoalkaloid antifungal of unknown mechanism/ergosterol biosynthesis | antifungal/membrane integrity | 28523 | no |
| Trichostatin A | 100 uM | chromatin regulation/HDACs | gene expression | 444732 | no |
| Trifluoperazine | 200 uM | signaling/calmodulin | signaling | 5566 | yes |
| Trimethoprim | 1.6 mg/ml | folate synthesis/DHFR | metabolism | 5578 | yes |
| Tunicamycin | 2.5 ug/ml | glycosylation/Alg7 | secretion | 11104835 | no |
| Usnic acid | 25 ug/ml | antimicrobial | antimicrobial | 6433557 | trials |
| Valinomycin | 20 uM | membrane integrity/potassium exclusion | membrane polarization | 5649 | no |
| Verrucarin | 5 uM | protein biosynthesis/polysome | protein turnover | 6437060 | no |
| ZnCl2 | 4 mM | metal homeostasis/diverse | diverse | 5727 | no |

A list of compounds used in this study, their targets, and the screening concentration.

deletions with the greatest number of phenotypes are *cnag_07622*Δ (encoding the COP9 signalosome subunit 1) and *cnag_05748*Δ (encoding a Nto1 subunit of the NuA3 histone acetyltransferase). Compounds that elicit the greatest number of responsive gene deletions (Figure 1F) are the heavy metal salt sodium tungstate and the trichothecene protein synthesis inhibitor verrucarin (Table S5), presumably reflecting the pleiotropic impact of these molecules on cells.

## Gene Ontology Analysis Reveals Processes Associated with Drug Sensitivity

Drug influx and efflux is thought to be a major general determinant of microbial drug susceptibility (Fernández and Hancock, 2012), but we also sought functions involved in drug sensitivity. We investigated this question in an unbiased fashion by analyzing chemogenomic profiles using Gene Ontology (GO), a gene annotation approach useful for comparative analyses. We first identified annotated orthologs of *C. neoformans* genes represented in the deletion library and associated GO terms with these orthologs. We then determined whether the sensitive gene knockouts that respond to each small molecule are enriched for association with particular GO terms relative to a randomized control set (Figure 2, Table S6). We observed that protein transport-related terms are highly enriched, as are processes related to ubiquitin modification/proteolysis and vesicle-mediated transport. These terms are associated with nine and five compounds, respectively, suggesting that intracellular transport and ubiquitin-mediated protein turnover may play important general roles in drug sensitivity.

## Comparison with *S. cerevisiae* Chemogenomic Profiling Data Sets

Chemogenomic profiling has been performed extensively in *S. cerevisiae*, allowing us to ask whether genetic responses to compounds were conserved. We performed a three-way comparison with two large-scale studies (Hillenmeyer et al., 2008; Parsons et al., 2006) (Figure 3A). Our data set has 46 compounds in common with Parsons et al. (2006) and 29 with Hillenmeyer et al. (2008); the two *S. cerevisiae* data sets had 15 compounds in common. First we identified genes whose knockouts exhibited a significant ($Z \leq -2.5$ or $\geq +2.5$) score (“responding”) when treated with a small molecule used in more than one data set, then identified which of those genes had orthologs in both *S. cerevisiae* and *C. neoformans*. We then calculated how many orthologs responded in both data sets. To adjust for a greater starting number of common genes when comparing the *S. cerevisiae* data sets to each other and control for functional biases, we limited this comparison to genes that also have orthologs in the *C. neoformans* knockout collection. The blue labels for compounds in Figures 3B–3D indicate statistically significant similarities ($p \leq 0.05$) in drug responses. Nearly all of the compounds in common between the two *S. cerevisiae* studies display statistically significant overlap in the genes that produced sensitivity to a given compound, despite the very different experimental platforms that were used to assess drug sensitivity/resistance (13/15 cases; Figure 3B). In striking contrast, few compounds show significantly conserved genetic responses when comparing either *S. cerevisiae* data set with the *C. neoformans* data. For the two *C. neoformans*-*S. cerevisiae* comparisons, only two of 46 compounds (Figure 3C) and one of 29 compounds (Figure 3D) show conserved responses, respectively.

The responses to azole compounds exhibit limited response conservation between species. Comparing our data set with Parsons et al., the responses to fluconazole (FLC) and clotrimazole, the azoles in both data sets, do not show significant overlap (Figure 3C). Likewise, between our data set and Hillenmeyer et al. (2008), no gene orthologs respond to miconazole and clotrimazole in both data sets (Figure 3D). In contrast, between the two *S. cerevisiae* data sets, the only shared azole, clotrimazole, shows a significantly similar response (Figure 3B). We compared published work that examined the transcriptome responses of *S. cerevisiae* (Kuo et al., 2010) and *C. neoformans* (Florio et al., 2011) to FLC. We found that, while there was significant overlap in orthologous genes impacted in the two species, ($p = 1.6 \times 10^{-3}$), there were also considerable differences: 67% of the genes with an altered response in *C. neoformans* whose orthologs in *S. cerevisiae* did not exhibit significant change, (Table S7) (Kuo et al., 2010).

## Using Chemical-Genetic Signatures to Identify Capsule Biosynthesis Mutants

Studies in *S. cerevisiae* have shown that that the phenotypic signatures of gene deletions for genes that act in the same process or protein complex tend to be similar (Collins et al., 2007; Costanzo et al., 2010; Nichols et al., 2011; Parsons et al., 2004; Parsons et al., 2006). We reasoned that this property of could be used in a pathogen to identify candidates for new genes involved in virulence by simply testing gene deletions that displayed phenotypic profiles similar to those corresponding to known virulence factors.

*C. neoformans* harbors an inducible polysaccharide capsule that is unusual among fungi (Del Poeta, 2004; Doering, 2009; Haynes et al., 2011; Kumar et al., 2011; O’Meara and Alspaugh, 2012; O’Meara et al., 2010; Vecchiarelli et al., 2013). The principal polysaccharide component, glucuronylxylomannan (GXM), consists of a repeating glycan unit that has α-1,3-linked mannose backbone with side chains of β-linked glucuronic acid and xylose (Kozel et al., 2003). Capsule production is critical for virulence and the ability of *C. neoformans* to evade detection and destruction by the host immune system (Vecchiarelli et al., 2013).

To identify candidates for genes involved in capsule formation and/or attachment, we organized our data set using hierarchical clustering of growth phenotypes produced by compound exposure. We focused on two clusters, each containing a gene(s) previously implicated in capsule biosynthesis: *PBX1* and *CPL1* (Liu et al., 2008; Liu et al., 2007b) in one cluster (Figure 4A) and *CAP60* (Chang and Kwon-Chung, 1998) in a second cluster (Figure 4B). The *pbx1*Δ/*cpl1*Δ cluster contains nine genes and the *cap60*Δ cluster seven. We quantified capsule accumulation after induction by computing the ratio of the diameter of the cell and capsule to the diameter of the cell alone (Figures 4C and 4D). Wild-type cells exhibit high capsule production, *pbx1*Δ mutants display a partial defect (Liu et al., 2007a) and *cpl1*Δ and *cap60*Δ mutants are acapsular (Chang and Kwon-Chung, 1998; Liu et al.,

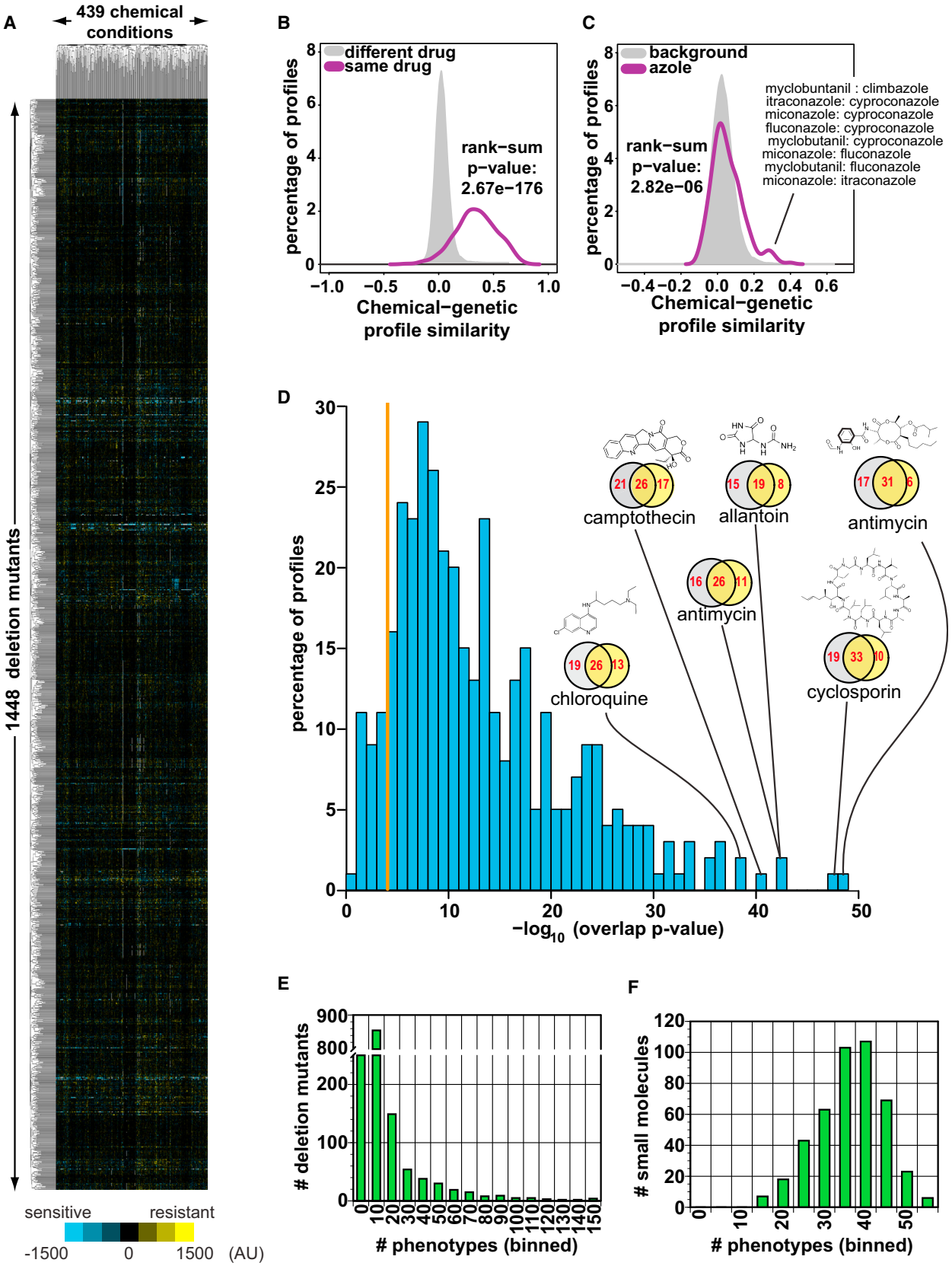


(legend on next page)

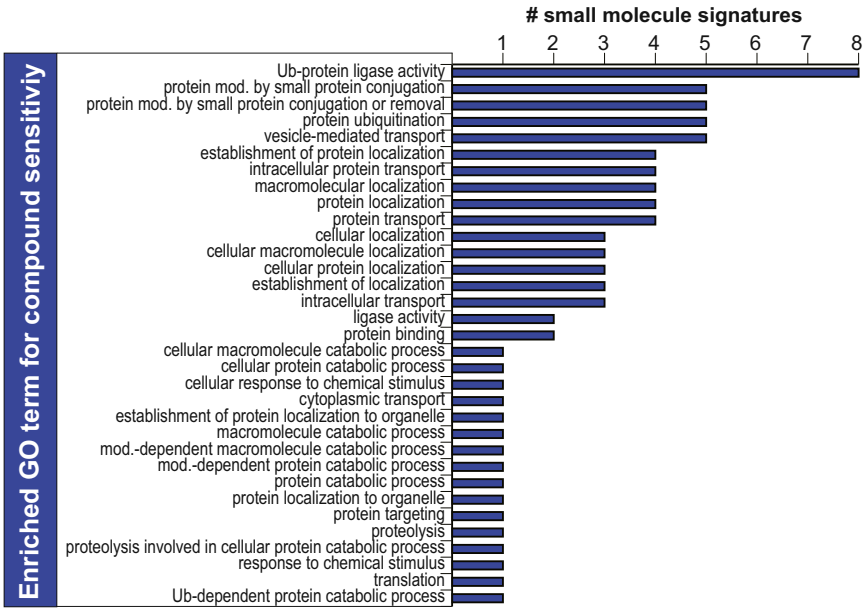


**Figure 2. Determinants of Compound Sensitivity**

We calculated whether molecules elicited a significant response from *C. neoformans* ORFs that are enriched for association with specific GO terms. Terms are listed on the y axis and the number of compounds whose responding gene knockouts associated with that GO term are listed on the x axis. See also Table S6.

2008). We found that seven of nine mutants in the *pbx1*Δ/*cpl1*Δ cluster exhibit a statistically significant capsule defect, as did four of the seven mutants in the *cap60*Δ cluster. In contrast, previous work from our laboratory found that approximately 1% of the original *C. neoformans* library shows a gross defect in capsule production (Liu et al., 2008).

Previous work showed that *pbx1*Δ mutants produce polysaccharide capsule whose attachment to the cell wall is sensitive to sonication, a finding that we confirmed (Figures 4C and 4D). We refer to the cell's ability to retain GXM on the cell surface as "capsule maintenance." Knockout mutants in *cnag_01058* do not exhibit a basal capsule defect but lost nearly 40% of their capsule diameter following sonication. Cells deleted for the *GCN5* gene, like *pbx1*Δ cells, show both decreased capsule levels and sonication-sensitive capsule. None of the mutants from the *cap60*Δ cluster produces a sonication-sensitive phenotype, suggesting that the *pbx1*Δ/*cpl1*Δ and *cap60*Δ clusters organize mutants that have distinct phenotypes. However, because several mutants do not produce visible capsule, the sonication test is insufficient to definitively measure capsule maintenance. We therefore analyzed how much glucoronoxylomannan (GXM), the major capsular polysaccharide (Doering, 2009), is secreted into the growth medium by blotting with α-GXM antibodies (Figure S2A). We found that two mutants that produce little (*gcn5*Δ) or no (*yap1*Δ) visible capsule still shed GXM into the medium, suggesting that they cannot retain capsule on their cell surface. Indeed, we found that they shed more GXM than *pbx1*Δ cells. Four of nine mutants in the *pbx1*Δ/*cpl1*Δ cluster exhibit a maintenance defect, whereas none of the *cap60*Δ cluster mutants do. We also found that GXM produced by these cells can be taken up and added to the surface ("donated") of an acapsular mutant using a standard GXM transfer assay (Kozel and Hermerath, 1984; Reese and Doering, 2003). Moreover, apparent capsule-defective mutants shed GXM (Figures S2B and S2C) and can donate GXM from conditioned medium (Figure S2C). Mutants that appear to not secrete GXM (*pbx1*Δ, *cpl1*Δ, and *sgf73*Δ) can donate it, but only if conditioned medium concentration is increased 10-fold (Figure S2D). These data are consistent with a recently published study on the role of Pbx1 in capsule attachment and assembly (Kumar et al., 2014).

Since the capsule is a major virulence trait of *C. neoformans*, we tested whether knockout mutants that exhibited a capsule defect displayed a defect in the mammalian host, using a murine inhalation model. We infected mice with a mixture of differentially-tagged wild-type and mutant cells at a ratio of 1:1. At 10 days

**Figure 1. Chemical-Genetic Profiling of *C. neoformans***

(A) Heat map of full data set following hierarchical clustering. Compounds are arrayed on the x axis and gene knockouts on the y axis. See also Tables S1 and S2.

(B) Probability density function for pairwise correlation scores between the chemical genetic profiles of different compounds (gray) and the same compounds at different concentrations (purple) screened on different days (different batches).Scores between the chemical-genetic profiles of different concentrations of the same compounds are significantly higher than those between different compounds (Wilcoxon test, $p = 2.7 \times 10^{-176}$). See also Figure S1.

(C) Probability density function for pairwise correlation scores between the chemical genetic profiles of different compounds (gray) and azole family compounds (purple). Pairwise comparisons between azoles exhibit higher correlation scores than nonazole compounds (Wilcoxon test, $p = 2.8 \times 10^{-6}$). Molecules with the highest pairwise comparisons scores are listed on the right.

(D) Pearson's correlation score between two different concentrations of the same compounds. Concentrations with similar correlation scores are binned together (y axis). For compounds with the greatest correlation scores between concentrations, Venn diagrams of significant genes ($Z < -2.5$) present in profiles from the same compounds at different concentrations and the small-molecule structure are shown. The orange line indicates a hypergeometric p value $\leq 0.05$

(E)Histogram showing the number of deletion mutants that have given number of phenotypes. A phenotype is considered $|Z| > 2.5$ and we identified phenotypes independently for each small-molecule concentration.

(F) Histogram showing the number of small molecules that have a given number of phenotypes. Phenotypes ($|Z| > 2.5$) were identified for each small-molecule condition/concentration

See also Figure S1 and Tables S1, S2, S3, S4, and S5.

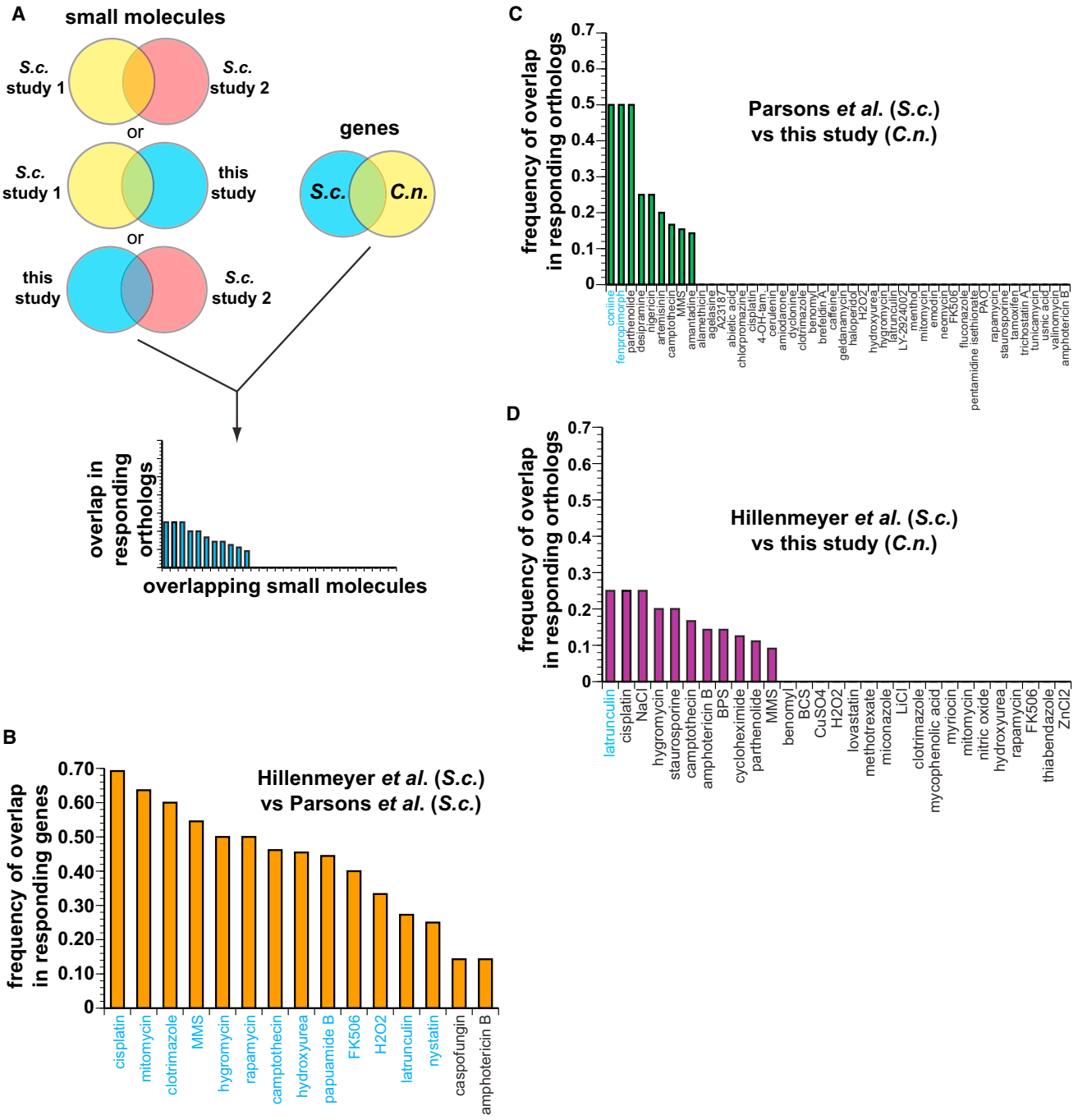


**Figure 3. Chemical-Genetic Signatures of *C. neoformans* Genes Differ from Orthologous *S. cerevisiae* Genes**

(A) Flowchart of computation process for comparing data sets. We identified *C. neoformans* and *S. cerevisiae* orthologous genes that were present in all data sets, then compared the responses of only those genes in all the data sets. We compared genes whose knockout mutants significantly ($|Z| > 2.5$) responded to compound that were common in at least two of the data sets.

(B) Comparison between Parsons et al. (2006) and Hillenmeyer et al. (2008), comparing the response ($|Z| > 2.5$) of genes that have orthologs present in the *C. neoformans* data set. Compounds whose profiles exhibit significant overlaps ($p < 0.05$) are labeled in blue.

(C) Comparison between our data set and Parsons et al. (2006) Compounds whose profiles exhibit significant overlaps ($p < 0.05$) are labeled in blue.

(D) Comparison between our data set and Hillenmeyer et al. (2008) Compounds whose profiles exhibit significant overlaps ($p < 0.05$) are labeled in blue.

postinfection (dpi), we sacrificed animals, harvested and homogenized lung tissue, then plated on the appropriate selective media for colony forming units (CFUs). All but one of the *pbx1*Δ/*cpl1*Δ cluster members were significantly underrepresented relative to wild-type; the exception was the *cnag_01058*Δ mutant, which is defective in capsule maintenance but not capsule biosynthesis (Figures 4C and S2A). *yap1*Δ cells, which appear acapsular but secrete GXM, displayed a major defect in fitness in the host (Figure 4E). Three of four *cap60*Δ cluster mutants also display a defect in accumulation of CFUs in host lungs (Figure 4E).

## Chemogenomics Identifies the Cell Cycle as a Target of the Antifungal Small Molecule S8

We included a number of drug-like antifungal compounds in our screen in order to identify their targets (Table 1). Our use of *C. neoformans* chemogenomics to assist in the identification of a target of toremifene is described elsewhere (Butts et al., 2014). Here we investigate the thiazolidine-2,4-dione derivatives originally described for their activity against *C. albicans* biofilms (Kagan et al., 2014).

Our chemogenomic profiling data of the thiazolidine-2,4-dione derivative S8 revealed a striking outlier: a knockout mutant in the gene coding for a *C. neoformans* ortholog of the conserved cell-cycle kinase Wee1, is relatively resistant (Figure 5A). We observed resistance at multiple concentrations of S8 (Table S2). The related compound NA8, which contains a replacement of a sulfur atom with a carbon atom on the thiazolidinedione moiety (Figure 5B), does not elicit the same resistance (Figure S3A). The *wee1*Δ mutant is also resistant to S10 (Figure S3B), which harbors a C10 alkyl chain instead of C8 but is otherwise identical to S8 (Figure S3C).

Wee1 regulates the G2/M cell-cycle checkpoint through inhibitory phosphorylation of Cdk1, which in turn is required for cells to traverse the checkpoint. The essential phosphatase Cdc25 activates Cdk1 by removing the inhibitory phosphorylation added by Wee1 (Morgan, 2007) (Figure 5C). Because the *wee1*Δ is relatively resistant to S8, we hypothesized that S8 targeted a protein that acts through Wee1 to regulate Cdk1. One such target could be Cdc25.

We reasoned that if the Wee1/Cdc25-regulated step of the cell cycle were an important target of S8 in vivo, wild-type *C. neoformans* cells treated with S8 would arrest at G2/M. To test this prediction, we treated exponential cultures with S8, S10, or NA8 and examined the impact on the cell cycle. We harvested and fixed representative samples every 30 min, then analyzed DNA content by flow cytometry. Control cultures treated with DMSO (carrier) (Figure 5D) or the control compound NA8 (Figure 5E) stayed asynchronous for the entire 3.5 hr of the time course. Strikingly, S8-treated (Figure 5F) cells accumulated with 2C DNA content, which indicates G2/M arrest in *C. neoformans*, a haploid yeast (Whelan and Kwon-Chung, 1986). At later time points, cells synthesize DNA but do not complete mitosis and cytokinesis. This is consistent with observations in *S. pombe* that partial inhibition of Cdk1 permits re-replication of DNA (Broek et al., 1991).

Because inhibition of Cdc25 would provide a parsimonious explanation for the genetic and biological properties of S8, we tested whether S8 inhibits *C. neoformans* Cdc25 in vitro. We expressed and purified the catalytic domain of a *C. neoformans* ortholog (*CNAG_07942*) in *E. coli* (Figure S3D) and then performed in vitro phosphatase assays using 3-O-methyl fluorescein phosphate (OMFP) as a substrate (Figures 5G and 5H) (Hill et al., 1968). We observed that S8 inhibits Cdc25 activity ($K_i$ ~140 μM, Figure 5E), as do both S10 (Figure S3E) and NSC 663284 ($K_i$~250 μM, Figure S3F), a commercially available inhibitor of mammalian Cdc25 (Pu et al., 2002). The control compound NA8 does not inhibit *C. neoformans* Cdc25 in vitro (Figure S3G). For S8, the in vitro inhibition constant is roughly comparable to the liquid MIC value against *C. neoformans*, which we measured to be ~60 μM in YNB. S10 has a higher $K_i$ ($K_i$~310 μM) but similar to the MIC value (~55 μM) measured in YNB agar compared to S8.

## O2M: A Genetic Biomarker Algorithm to Predict Compound Synergies

Drug resistance is a major clinical challenge in the treatment of both bacterial and fungal infections (Anderson, 2005; Cantas et al., 2013). An effective therapeutic strategy is to treat patients with drugs that act synergistically, enhancing each other's effectiveness beyond that produced by the sum of each drug's individual impact (Kalan and Wright, 2011). This approach is thought to decrease acquisition drug resistance, increase the available drug repertoire (Kalan and Wright, 2011) and ameliorate toxicities (Kathiravan et al., 2012; Lehár et al., 2009).

We hypothesized that we could use the chemogenomic information from our screens of drugs known to act synergistically, such as FLC and fenpropimorph (Jansen et al., 2009), to identify new synergistic interactions (Figure 6A). When we compared the identity of genes whose knockouts "responded" to each individual small molecule in a known synergistic pair ($|Z| \geq 2.5$, Tables S3 and S4), we found that this "responsive" gene set was significantly enriched over the expected value (Fisher's exact test, $p \leq 6 \times 10^{-5}$) (Figure 6A, top). This observation is consistent with a previous report that the chemical-genetic response to each drug in a synergistic pair is enriched for overlapping genes (Jansen et al., 2009).

This overlap in responsive gene sets led us to consider the possibility that overlapping responsive genes from known synergistic compound pairs could be used as biomarkers to predict new synergistic combinations. Our method involves first identifying the overlaps in responsive gene sets for all compounds that had been reported in the literature to synergize with a small molecule of interest ("compound X"), selecting those genes common to all of those sets (Figure 6A, middle, the overlaps of overlaps). We refer to these genes as "synergy biomarker genes." Critically, we next hypothesized that any compound that contains one or more of these synergy biomarker genes in its responsive gene set would be synergistic with compound X. Because our method used the overlaps of response gene overlaps between compounds known to be synergistic, we refer to it as the "overlap-squared method" or "O2M."

We then tested O2M using two drugs for which substantial literature synergy information was available: FLC and geldanamycin (GdA). FLC is an approved antifungal drug. GdA is an inhibitor of Hsp90, a chaperone protein with many physical and genetic interactions (Taipale et al., 2010). We performed our analysis on fenpropimorph and sertraline, which are known to

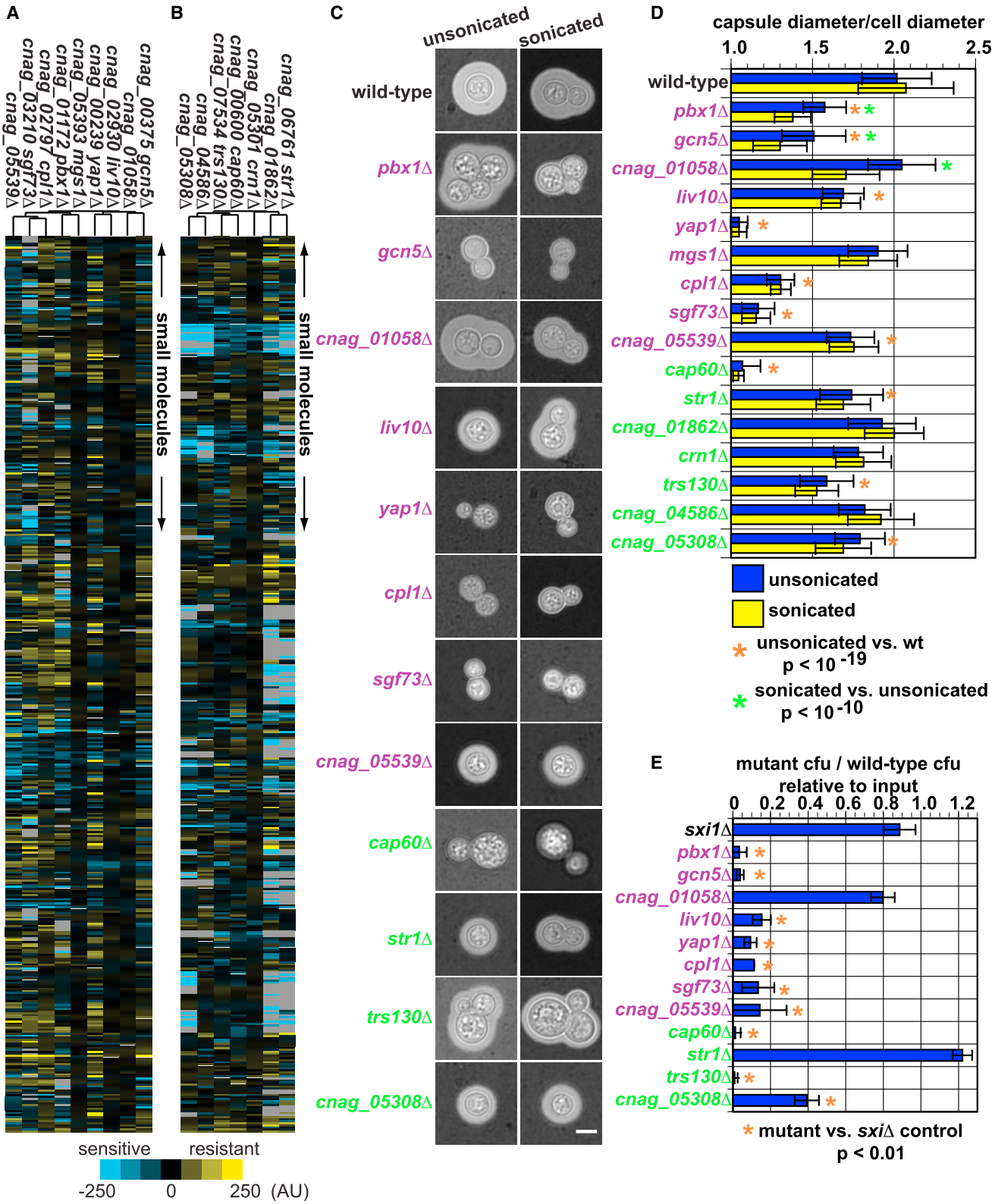


**Figure 4. Chemical-Genetic Profiling Identifies Genes Involved in Capsule Biosynthesis**

(A) Cluster containing the chemical signatures of the *pbx1*Δ and *cpl1*Δ mutants.

(B) Cluster containing the chemical signatures of the *cap60*Δ mutants.

*(legend continued on next page)*

act synergistically with FLC (Jansen et al., 2009; Zhai et al., 2012), and cyclosporine and rapamycin, which are known to act synergistically with GdA (Francis et al., 2006; Kumar et al., 2005). Using this prior knowledge and our data, we identified synergy biomarker genes for FLC (*CNAG_00573*, *CNAG_03664*, and *CNAG_03917*) and GdA (*CNAG_01172*, *CNAG_03829*, and *CNAG_01862*). We generated a list of compounds from our chemical-genetics data set that contain one or more of these genes in their responsive genes set.

We then used a standard ''checkerboard'' assay to experimentally determine fractional inhibitory concentration index (FICI), and we adopted the standard that an FICI value below 0.5 is synergistic (Meletiadis et al., 2010). We determined FICIs for FLC and GdA with three sets of compounds: (1) the compounds predicted from synergy biomarker genes, (2) the predicted synergistic compounds for the other drug (e.g., we tested compounds predicted to be synergistic with GdA for synergy with FLC), and (3) a randomly generated subset of the compounds not predicted to act synergistically with either FLC or GdA. The second and third groups are as controls for compounds that are generally synergistic and to determine the background frequency of synergistic interactions within a set of compounds.

Respective experimental FICI values for FLC and GdA are shown in Figures 6B and 6C (yellow bars: synergy; blue bars additive or worse interactions). The labels for compounds we predicted to be synergistic are colored purple, positive controls (published synergistic compound pairs) are colored green, and predicted negative control compounds are colored blue (Figure 6). We observed that only ~10% of the negative control compounds act synergistically with either FLC or GdA. In striking contrast, we found ~80% and ~60% of the compounds selected by O2M are synergistic with FLC and GdA, respectively. Thus, for two unrelated compounds, O2M is highly successful at predicting synergistic interactions and performs vastly better than the brute force trial-and-error approach (Figures 6D and 6E) ($p < 0.0008$, Fisher's exact test).

## DISCUSSION

We applied chemogenomic profiling to the major fungal driver of AIDS-related death, the encapsulated yeast *C. neoformans,* to produce a chemical-genetic atlas of this important pathogen. Beyond identifying new virulence factors and compound mode of action, we describe a conceptually general approach to identifying drug synergies that combines prior knowledge and chemogenomic profiles.

### A Chemical-Genetic Atlas for *C. neoformans*

We maximized the quality of the atlas in several ways. To capture concentration-dependent impacts of compounds, we obtained the MIC for each compound and examined the genetic responses at multiple concentrations below MIC. In addition, we performed a large number of control screens and incorporated batch information for systematic correction. Overall benchmarks of data quality (Figure 1) together with nearest neighbor and Gene Ontology analysis (Figure 2) support the existence of substantial chemical-genetic signal in the data. Even genes with orthologs in both *S. cerevisiae* and *C. neoformans* show considerable differences in responses (Figure 3). While this may not be surprising given the large phylogenetic distance between these fungi, it shows that understanding the chemical responses of pathogens requires pathogen-focused studies, even when considering conserved genes and processes. For example, we observed differences in the responses to azole drugs between *S. cerevisiae* and *C. neoformans* (Figure 3). Since azoles are heavily used clinically, differences in responses between species are of significant interest.

### Insights Gained from Initial Use of the *C. neoformans* Chemical-Genetic Atlas

#### *Identification of Mutants that Impact Capsule Formation and Mammalian Infection*

Our studies on capsule biosynthesis genes focused two different clusters that contained genes that we and others have shown to be required for capsule formation, the *pbx1/cpl1Δ* cluster and the *cap60Δ* cluster. As anticipated from model organism studies (Collins et al., 2007; Costanzo et al., 2010; Nichols et al., 2011; Parsons et al., 2004; Parsons et al., 2006), these clusters were indeed enriched for genes whose mutants are defective in capsule biosynthesis and mammalian pathogenesis. The genes represented by the two clusters differed functionally in that genes in the *pbx1/cpl1Δ* cluster but not the *cap60Δ* cluster are required for association of capsule polysaccharide with the cell surface (Figures 4 and S2). A recent study on Pbx1 and its ortholog, Pbx2, proposes that the two proteins act redundantly in capsule assembly (Kumar et al., 2014). *pbx1*Δ and *pbx2*Δ cells shed lower amounts of GXM into the culture medium but that the GXM functions in a capsule transfer assay. Electron microscopy studies indicate that these mutants exhibit defects in the cell wall. Our data are fully consistent with these data. Other genes from the *pbx1Δ/cpl1Δ* cluster likely play a role in these processes. Some, like *GCN5* and *SGF73*, which encode orthologs of the yeast SAGA histone acetylase/deubiquitylase complex, are clearly regulatory, while others could act more directly. While detailed validation and investigation of these many candidates (including gene deletion reconstruction studies) will be required to obtain mechanistic insight into capsule biology, their enrichment suggests value of this Cryptococcal chemogenomic resource in identifying mutants defective in virulence.

#### *Compound Target Identification*

Chemogenomic profiling has proven useful in identifying targets of uncharacterized compounds (Parsons et al., 2006), including

(C) Images of individual cells grown in 10% Sabouraud's broth to induce capsule. Representative cells are shown for mutants that exhibit a statistically significant phenotype. Scale bar, 5 μm.

(D) Quantification of capsule sizes from all mutants in *pbx1*Δ/*cpl1*Δ (purple labels) cluster or *cap60*Δ (green labels) cluster. 100 cells were measured for each strain, the error bars represents the standard deviation, and p values were calculated using Student's t test.

(E) Colony counts from colony forming units (cfu) extracted from mouse lungs following an inhalation infection. Three mice are shown for each datapoint; the error bars represent the standard deviation and p values were calculated using Student's t test.

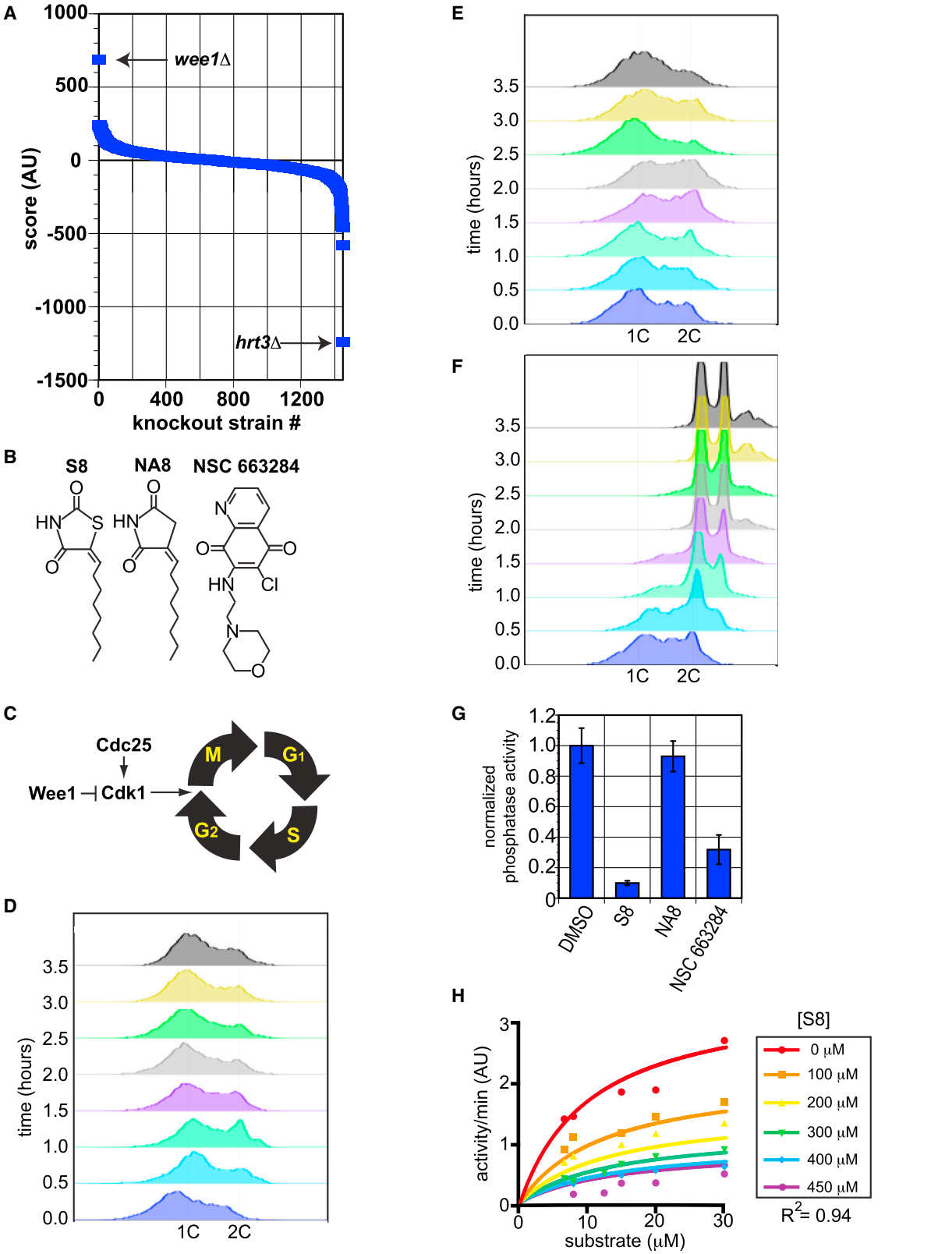


(legend on next page)

in the pathogenic fungus *C. albicans* (Jiang et al., 2008; Xu et al., 2007; Xu et al., 2009). Chemical-genetic data can be used to determine the target of compounds within complex mixtures (Jiang et al., 2008; Xu et al., 2009). Our goal differed: we sought to identify targets of repurposed compounds, as described elsewhere (Butts et al., 2013), or, in the case of S8, a compound identified as an inhibitor of *Candida* biofilms (Kagan et al., 2014). The identification of the Wee1 kinase as a sensitivity determinant for S8, the cell-cycle arrest produced by S8, and the ability of the compound to inhibit *Cn*Cdc25 in vitro together support the model that S8 inhibits growth through via the cell cycle at least in part via inhibition of Cdc25. Whether this explains its impact on biofilms requires further investigation. As with any compound target, ultimate proof that Cdc25 is the target of S8 will require the isolation of resistance alleles of *CDC25*.

Given the simplicity of the pharmacophore and its $K_i$ for *Cn*Cdc25, it would not be surprising if S8 had additional cellular targets, as recently described (Feldman et al., 2014). Cdc25 is a conserved cell-cycle phosphatase and therefore might be considered a poor drug target a priori but cyclin-dependent kinases are a focus of recent antiparasite therapeutics (Geyer et al., 2005). It is also notable that the target of azole antifungals, lanosterol 14-demethylase (Ghannoum and Rice, 1999) is conserved from yeast to human.

### *O2M: Predicting Compound Synergies Using Prior Knowledge and Chemical Profiles*

Identifying synergistic drug interactions is of considerable clinical interest, but efficient methods for their identification are elusive. Systematic examination of combinations of a small set of compounds using *S. cerevisiae* suggests that synergies are relatively rare and often involve so-called "promiscuous" synergizers, compounds that are synergistic with multiple partners (Cokol et al., 2011). Chemogenomic studies have shown that drugs known to be synergistic tend to have overlapping "responding" gene sets (Jansen et al., 2009). We expanded on this concept to develop a highly parallel method, O2M, for efficiently predicting synergistic drug interactions. Our work utilizes prior knowledge of drug synergies to identify a discrete set of predictive biomarker genes for a given compound. We experimentally demonstrated the utility of O2M for two compounds, FLC and geldanamycin. Our method identified dozens of synergistic interactions and discovered a small number of biomarkers that could serve as readouts for further screens for synergistic drugs. The method appears to not simply select promiscuous synergiziers: five of six drugs previously classified as promiscuous synergizers (Cokol et al., 2011) were tested in our studies but most were not predicted to be synergistic by O2M. One of the promiscuous compounds was a positive control (fenpropimorph with FLC) and another (dyclonine) was predicted synergistic with FLC but was not and was predicted not synergistic with GdA but was. We anticipate that O2M could be used to identify synergistic compound interactions in published *E. coli* and *C. albicans* chemical-genetics data sets (Jiang et al., 2008; Nichols et al., 2011; Xu et al., 2007; Xu et al., 2009).

## EXPERIMENTAL PROCEDURES

### Determination of MICs

We determined MIC on solid growth medium for each compound used in screening (Table 1).

### Colony Array-Based Chemogenomic Profiling

*C. neoformans* knockouts were inoculated from frozen 384-well plates to YNB + 2% glucose. Plates were grown 24 hr at 30°C, then used to inoculate screening plates containing compounds of interest.

### Data Analysis

Data were analyzed as previously described (Baryshnikova et al., 2010) with the a few exceptions.

### *C. neoformans* Ortholog Identification and GO Term Mapping

Mapping from *S. cerevisiae* Uniprot Proteins to *C. neoformans* Uniprot Proteins was done using One-to-one mappings in MetaPhOrs (http://metaphors.phylomedb.org/). *C. neoformans* ORFs were compared to a database of *S. cerevisiae* Uniprot Proteins using blastp (Altschul et al., 1997) with a E-score cutoff of $10^{-30}$. Corresponding yeast GO annotations were mapped onto the *C. neoformans* ORFs.

### Comparison of Transcriptional Response to FLC

Compared transcriptional responses between *S. cerevisiae* (Kuo et al., 2010) and *C. neoformans* (Florio et al., 2011).

### Capsule Induction Assay

Samples were grown overnight at 30°C in 100% Sabouraud's broth, then diluted 1:100 into 10% Sabouraud's broth buffered with 50 mM HEPES pH 7.3 and grown for 3 days at 37°C. India ink was added at 3:1 ratio and samples imaged on a Zeiss Axiovert microscope.

### Capsule Transfer Assay

Performed as in (Reese and Doering, 2003), with minor modifications.

### GXM Immunoblot Assay

Conditioned medium was made from donor GXM donor strains as described above.

**Figure 5. *C. neoformans* Cdc25 Is a Target of S8 In Vivo and In Vitro**

(A) Chemical-genetic data of the growth scores of each knockout mutant grown on S8 (y axis). The mutant that exhibited the greatest resistance is *wee1*Δ. The mutant strain that showed the greatest sensitivity to S8 is *cnag_04462*Δ.

(B) Structures of S8, NA8, and NSC 663284. The structure of S10 is shown in Figure S3C.

(C) G2/M regulation (Morgan, 2007).

(D) DNA content of asynchronous *C. neoformans* culture split into aliquots for treatment with compounds of interest, with samples harvested at appropriate times. Data for DMSO-treated culture is shown.

(E) DNA content from NA8-treated culture from same starting culture as Figure 5F.

(F) DNA content from S8-treated culture from same starting culture as Figure 5F.

(G) Phosphatase activity of purified C. neoformans Cdc25 catalytic domain (CNAG_01572, aa442-662). Average of three independent replicates are shown and the error bars represent the standard deviation.

(H) Michaelis-Menten kinetics of S8 inhibition of *Cn*Cdc25 from in vitro phosphatase activity. A noncompetitive model of enzyme inhibition produced the best $R^2$ value (0.94).

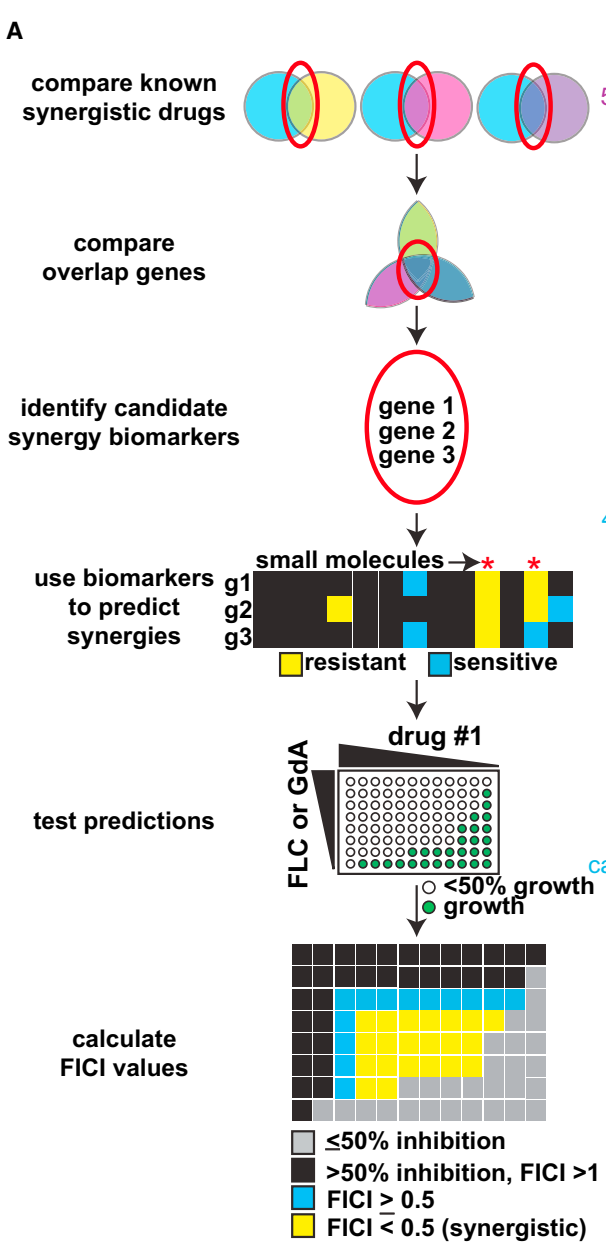


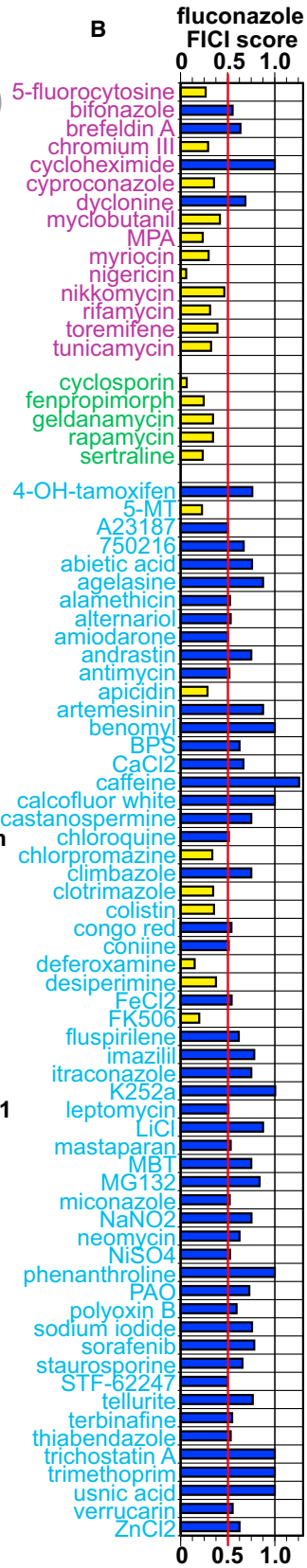


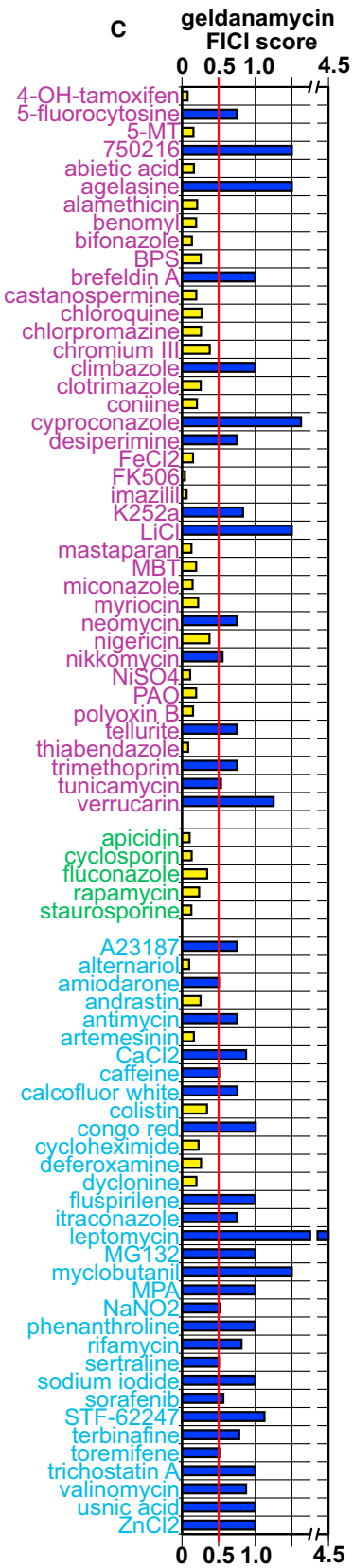


D

| fluconazole | predicted synergistic | negative controls |
|---|---|---|
| synergistic | 11 | 8 |
| not synergistic | 4 | 50 |

E

| geldanamycin | predicted synergistic | negative controls |
|---|---|---|
| synergistic | 25 | 6 |
| not synergistic | 15 | 26 |

(legend on next page)

### Mouse Infection Assay

Mouse lung infections were performed as previously described (Chun et al., 2011).

### Cdc25 Protein Purification

We identified the *C.* neoformans ortholog of Cdc25, *CNAG_01572*, by best reciprocal BLAST (Altschul et al., 1997) hit with the human Cdc25A, Cdc25B, and Cdc25C protein isoforms. We then inserted the exonic sequence of the catalytic domain into a 6×-His tag expression vector for purification.

### Cdc25 Phosphatase Assay

Cdc25 phosphatase activity was analyzed in activity buffer (50 mM Tris pH 8.3, 5% glycerol, 0.8 mM dithiolthreitol, and 1% PVA).

### Cdc25 Inhibitor Treatment and FACS Analysis

Wild-type *C. neoformans* was grown overnight in 1× YNB at 30°C with rotation. Cultures were diluted to $OD_{600}$ ~0.2 into 150 ml 1× YNB, then incubated 3 hr at 30°C. Samples were then split and NA8, S8, and S10 added to 60 μM. Equivalent volume of DMSO was added to the control culture.

### Fractional Inhibitory Concentration Index Assay for Synergy

We determined FICI using a standard checkerboard assay (Hsieh et al., 1993), calculating FICI as described using a 50% growth inhibition cutoff for MICs for individual compounds (Hsieh et al., 1993; Meletiadis et al., 2010), then using a standard cutoff of FICI < 0.5 to define synergy.

See Extended Experimental Procedures for additional details.

## SUPPLEMENTAL INFORMATION

Supplemental Information includes Extended Experimental Procedures, three figures, and seven tables and can be found with this article online at http://dx.doi.org/10.1016/j.cell.2014.10.044.

## AUTHOR CONTRIBUTIONS

J.C.S.B. and H.D.M. designed the study. J.C.S.B. carried out all of experiments described in the paper. J.N. and C.L.M. performed data analysis shown in Figures 1B–1D, Figure 2 and Figure 3. B.V., R.D., and C.L.M. filtered, denoised and scored the primary colony array data. A.B., S.K., I.P., and D.J.K. provided compounds and guidance. J.C.S.B. and H.D.M. wrote the manuscript with input from all coauthors.

## ACKNOWLEDGMENTS

This work was supported by NIH grants 5R01AI099206 to H.D.M., 1R01AI091422 to D.J.K., 1R01HG005084 and 1R01GM04975 to C.L.M, and a grant from the CIFAR Genetic Networks Program to C.L.M.

Received: July 3, 2014
Revised: August 28, 2014
Accepted: October 22, 2014
Published: November 20, 2014

## REFERENCES

Altschul, S.F., Madden, T.L., Schäffer, A.A., Zhang, J., Zhang, Z., Miller, W., and Lipman, D.J. (1997). Gapped BLAST and PSI-BLAST: a new generation of protein database search programs. Nucleic Acids Res. *25*, 3389–3402.

Anderson, J.B. (2005). Evolution of antifungal-drug resistance: mechanisms and pathogen fitness. Nat. Rev. Microbiol. *3*, 547–556.

Armstrong-James, D., Meintjes, G., and Brown, G.D. (2014). A neglected epidemic: fungal infections in HIV/AIDS. Trends Microbiol. *22*, 120–127.

Baryshnikova, A., Costanzo, M., Kim, Y., Ding, H., Koh, J., Toufighi, K., Youn, J.-Y., Ou, J., San Luis, B.-J., Bandyopadhyay, S., et al. (2010). Quantitative analysis of fitness and genetic interactions in yeast on a genome scale. Nat. Methods *7*, 1017–1024.

Broek, D., Bartlett, R., Crawford, K., and Nurse, P. (1991). Involvement of p34cdc2 in establishing the dependency of S phase on mitosis. Nature *349*, 388–393.

Butts, A., and Krysan, D.J. (2012). Antifungal drug discovery: something old and something new. PLoS Pathog. *8*, e1002870.

Butts, A., DiDone, L., Koselny, K., Baxter, B.K., Chabrier-Rosello, Y., Wellington, M., and Krysan, D.J. (2013). A repurposing approach identifies off-patent drugs with fungicidal cryptococcal activity, a common structural chemotype, and pharmacological properties relevant to the treatment of cryptococcosis. Eukaryot. Cell *12*, 278–287.

Butts, A., Koselny, K., Chabrier-Roselló, Y., Semighini, C.P., Brown, J.C.S., Wang, X., Annadurai, S., DiDone, L., Tabroff, J., Childers, W.E., Jr., et al. (2014). Estrogen receptor antagonists are anti-cryptococcal agents that directly bind EF hand proteins and synergize with fluconazole in vivo. MBio *5*, e00765–e13.

Cantas, L., Shah, S.Q.A., Cavaco, L.M., Manaia, C.M., Walsh, F., Popowska, M., Garelick, H., Bürgmann, H., and Sørum, H. (2013). A brief multi-disciplinary review on antimicrobial resistance in medicine and its linkage to the global environmental microbiota. Front Microbiol *4*, 96.

Chang, Y.C., and Kwon-Chung, K.J. (1998). Isolation of the third capsule-associated gene, CAP60, required for virulence in Cryptococcus neoformans. Infect. Immun. *66*, 2230–2236.

Chun, C.D., Brown, J.C.S., and Madhani, H.D. (2011). A major role for capsule-independent phagocytosis-inhibitory mechanisms in mammalian infection by Cryptococcus neoformans. Cell Host Microbe *9*, 243–251.

Cokol, M., Chua, H.N., Tasan, M., Mutlu, B., Weinstein, Z.B., Suzuki, Y., Nergiz, M.E., Costanzo, M., Baryshnikova, A., Giaever, G., et al. (2011). Systematic exploration of synergistic drug pairs. Mol. Syst. Biol. *7*, 544.

Collins, S.R., Miller, K.M., Maas, N.L., Roguev, A., Fillingham, J., Chu, C.S., Schuldiner, M., Gebbia, M., Recht, J., Shales, M., et al. (2007). Functional dissection of protein complexes involved in yeast chromosome biology using a genetic interaction map. Nature *446*, 806–810.

Costanzo, M., Baryshnikova, A., Bellay, J., Kim, Y., Spear, E.D., Sevier, C.S., Ding, H., Koh, J.L.Y., Toufighi, K., Mostafavi, S., et al. (2010). The genetic landscape of a cell. Science *327*, 425–431.

Del Poeta, M. (2004). Role of phagocytosis in the virulence of Cryptococcus neoformans. Eukaryot. Cell *3*, 1067–1075.

**Figure 6. O2M Approach for Predicting Compound Synergy**

(A) Approach for predicting compound synergistic interaction.

(B) FICI values for fluconazole (FLC). Predicted synergistic compounds are labeled in purple and known synergistic compounds in green. Bars represent the average of two assays but both had to be FICI < 0.5 to be considered synergistic. Compounds labeled in blue are negative controls from one of two categories: 1) predicted to synergize with geldanamycin (GdA) but not FLC or 2) randomly generated list of compounds not predicted to be synergistic with either FLC or GdA. Yellow bars represent an FICI < 0.5 (synergistic) and blue bars and FICI ≥ 0.5 (not synergistic).

(C) FICI values for GdA. Labels and colors are analogous to those in part B.

(D) Contingency table of synergistic versus nonsynergistic interactions with FLC. $p < 0.0008$ (Fisher's exact test).

(E) Contingency table of synergistic versus nonsynergistic interactions with GdA. $p < 0.0008$ (Fisher's exact test).

Dittmar, J.C., Reid, R.J., and Rothstein, R. (2010). ScreenMill: a freely available software suite for growth measurement, analysis and visualization of high-throughput screen data. BMC Bioinformatics *11*, 353–363.

Doering, T.L. (2009). How sweet it is! Cell wall biogenesis and polysaccharide capsule formation in Cryptococcus neoformans. Annu. Rev. Microbiol. *63*, 223–247.

Feldman, M., Al-Quntar, A., Polacheck, I., Friedman, M., and Steinberg, D. (2014). Therapeutic potential of thiazolidinedione-8 as an antibiofilm agent against *Candida albicans*. PLoS ONE *9*, e93225.

Fernández, L., and Hancock, R.E.W. (2012). Adaptive and mutational resistance: role of porins and efflux pumps in drug resistance. Clin. Microbiol. Rev. *25*, 661–681.

Florio, A.R., Ferrari, S., De Carolis, E., Torelli, R., Fadda, G., Sanguinetti, M., Sanglard, D., and Posteraro, B. (2011). Genome-wide expression profiling of the response to short-term exposure to fluconazole in Cryptococcus neoformans serotype A. BMC Microbiol. *11*, 97.

Francis, L.K., Alsayed, Y., Leleu, X., Jia, X., Singha, U.K., Anderson, J., Timm, M., Ngo, H., Lu, G., Huston, A., et al. (2006). Combination mammalian target of rapamycin inhibitor rapamycin and HSP90 inhibitor 17-allylamino-17-demethoxygeldanamycin has synergistic activity in multiple myeloma. Clin. Cancer Res. *12*, 6826–6835.

Geyer, J.A., Prigge, S.T., and Waters, N.C. (2005). Targeting malaria with specific CDK inhibitors. Biochim. Biophys. Acta *1754*, 160–170.

Ghannoum, M.A., and Rice, L.B. (1999). Antifungal agents: mode of action, mechanisms of resistance, and correlation of these mechanisms with bacterial resistance. Clin. Microbiol. Rev. *12*, 501–517.

Haynes, B.C., Skowyra, M.L., Spencer, S.J., Gish, S.R., Williams, M., Held, E.P., Brent, M.R., and Doering, T.L. (2011). Toward an integrated model of capsule regulation in *Cryptococcus neoformans*. PLoS Pathog. *7*, e1002411.

Heitman J., Kozel T.R., Kwon-Chung K.J., Perfect J.R., and Casadevall A., eds. (2011). Cryptococcus: from human pathogen to model yeast (Washington, D.C.: ASM Press).

Hill, H.D., Summer, G.K., and Waters, M.D. (1968). An automated fluorometric assay for alkaline phosphatase using 3-O-methylfluorescein phosphate. Anal. Biochem. *24*, 9–17.

Hillenmeyer, M.E., Fung, E., Wildenhain, J., Pierce, S.E., Hoon, S., Lee, W., Proctor, M., St Onge, R.P., Tyers, M., Koller, D., et al. (2008). The chemical genomic portrait of yeast: uncovering a phenotype for all genes. Science *320*, 362–365.

Hsieh, M.H., Yu, C.M., Yu, V.L., and Chow, J.W. (1993). Synergy assessed by checkerboard. A critical analysis. Diagn. Microbiol. Infect. Dis. *16*, 343–349.

Janbon, G., Ormerod, K.L., Paulet, D., Byrnes, E.J., 3rd, Yadav, V., Chatterjee, G., Mullapudi, N., Hon, C.-C., Billmyre, R.B., Brunel, F., et al. (2014). Analysis of the genome and transcriptome of *Cryptococcus neoformans* var. *grubii* reveals complex RNA expression and microevolution leading to virulence attenuation. PLoS Genet. *10*, e1004261.

Jansen, G., Lee, A.Y., Epp, E., Fredette, A., Surprenant, J., Harcus, D., Scott, M., Tan, E., Nishimura, T., Whiteway, M., et al. (2009). Chemogenomic profiling predicts antifungal synergies. Mol. Syst. Biol. *5*, 338.

Jiang, B., Xu, D., Allocco, J., Parish, C., Davison, J., Veillette, K., Sillaots, S., Hu, W., Rodriguez-Suarez, R., Trosok, S., et al. (2008). PAP inhibitor with in vivo efficacy identified by Candida albicans genetic profiling of natural products. Chem. Biol. *15*, 363–374.

Kagan, S., Jabbour, A., Sionov, E., Alquntar, A.A., Steinberg, D., Srebnik, M., Nir-Paz, R., Weiss, A., and Polacheck, I. (2014). Anti-Candida albicans biofilm effect of novel heterocyclic compounds. J. Antimicrob. Chemother. *69*, 416–427.

Kalan, L., and Wright, G.D. (2011). Antibiotic adjuvants: multicomponent anti-infective strategies. Expert Rev. Mol. Med. *13*, e5.

Kathiravan, M.K., Salake, A.B., Chothe, A.S., Dudhe, P.B., Watode, R.P., Mukta, M.S., and Gadhwe, S. (2012). The biology and chemistry of antifungal agents: a review. Bioorg. Med. Chem. *20*, 5678–5698.

Kozel, T.R., and Hermerath, C.A. (1984). Binding of cryptococcal polysaccharide to Cryptococcus neoformans. Infect. Immun. *43*, 879–886.

Kozel, T.R., Levitz, S.M., Dromer, F., Gates, M.A., Thorkildson, P., and Janbon, G. (2003). Antigenic and biological characteristics of mutant strains of Cryptococcus neoformans lacking capsular O acetylation or xylosyl side chains. Infect. Immun. *71*, 2868–2875.

Kumar, R., Musiyenko, A., and Barik, S. (2005). Plasmodium falciparum calcineurin and its association with heat shock protein 90: mechanisms for the antimalarial activity of cyclosporin A and synergism with geldanamycin. Mol. Biochem. Parasitol. *141*, 29–37.

Kumar, P., Yang, M., Haynes, B.C., Skowyra, M.L., and Doering, T.L. (2011). Emerging themes in cryptococcal capsule synthesis. Curr. Opin. Struct. Biol. *21*, 597–602.

Kumar, P., Heiss, C., Santiago-Tirado, F.H., Black, I., Azadi, P., and Doering, T.L. (2014). Pbx proteins in Cryptococcus neoformans cell wall remodeling and capsule assembly. Eukaryot. Cell *13*, 560–571.

Kuo, D., Tan, K., Zinman, G., Ravasi, T., Bar-Joseph, Z., and Ideker, T. (2010). Evolutionary divergence in the fungal response to fluconazole revealed by soft clustering. Genome Biol. *11*, R77.

Lehár, J., Krueger, A.S., Avery, W., Heilbut, A.M., Johansen, L.M., Price, E.R., Rickles, R.J., Short, G.F., 3rd, Staunton, J.E., Jin, X., et al. (2009). Synergistic drug combinations tend to improve therapeutically relevant selectivity. Nat. Biotechnol. *27*, 659–666.

Liu, C., Apodaca, J., Davis, L.E., and Rao, H. (2007a). Proteasome inhibition in wild-type yeast *Saccharomyces cerevisiae* cells. Biotechniques *42*, 158–162, 160, 162.

Liu, O.W., Kelly, M.J.S., Chow, E.D., and Madhani, H.D. (2007b). Parallel β-helix proteins required for accurate capsule polysaccharide synthesis and virulence in the yeast Cryptococcus neoformans. Eukaryot. Cell *6*, 630–640.

Liu, O.W., Chun, C.D., Chow, E.D., Chen, C., Madhani, H.D., and Noble, S.M. (2008). Systematic genetic analysis of virulence in the human fungal pathogen *Cryptococcus neoformans*. Cell *135*, 174–188.

Loyse, A., Bicanic, T., and Jarvis, J.N. (2013). Combination antifungal therapy for cryptococcal meningitis. N. Engl. J. Med. *368*, 2522–2523.

Lozano, R., Naghavi, M., Foreman, K., Lim, S., Shibuya, K., Aboyans, V., Abraham, J., Adair, T., Aggarwal, R., Ahn, S.Y., et al. (2012). Global and regional mortality from 235 causes of death for 20 age groups in 1990 and 2010: a systematic analysis for the Global Burden of Disease Study 2010. Lancet *380*, 2095–2128.

Mandell, G.L., Bennett, J.E., and Dolin, R. (2010). Mandell, Douglas, and Bennett's Principles and Practice of Infectious Diseases, 7th edn (Philadelphia: Churchill Livingstone Elsevier).

Meletiadis, J., Pournaras, S., Roilides, E., and Walsh, T.J. (2010). Defining fractional inhibitory concentration index cutoffs for additive interactions based on self-drug additive combinations, Monte Carlo simulation analysis, and in vitro-in vivo correlation data for antifungal drug combinations against Aspergillus fumigatus. Antimicrob. Agents Chemother. *54*, 602–609.

Morgan, D.O. (2007). The Cell Cycle: Principles of Control (London, UK: New Science Press).

Nichols, R.J., Sen, S., Choo, Y.J., Beltrao, P., Zietek, M., Chaba, R., Lee, S., Kazmierczak, K.M., Lee, K.J., Wong, A., et al. (2011). Phenotypic landscape of a bacterial cell. Cell *144*, 143–156.

O'Meara, T.R., and Alspaugh, J.A. (2012). The Cryptococcus neoformans capsule: a sword and a shield. Clin. Microbiol. Rev. *25*, 387–408.

O'Meara, T.R., Norton, D., Price, M.S., Hay, C., Clements, M.F., Nichols, C.B., and Alspaugh, J.A. (2010). Interaction of Cryptococcus neoformans Rim101 and protein kinase A regulates capsule. PLoS Pathog. *6*, e1000776.

Park, B.J., Wannemuehler, K.A., Marston, B.J., Govender, N., Pappas, P.G., and Chiller, T.M. (2009). Estimation of the current global burden of cryptococcal meningitis among persons living with HIV/AIDS. AIDS *23*, 525–530.

Parsons, A.B., Brost, R.L., Ding, H., Li, Z., Zhang, C., Sheikh, B., Brown, G.W., Kane, P.M., Hughes, T.R., and Boone, C. (2004). Integration of chemical-genetic and genetic interaction data links bioactive compounds to cellular target pathways. Nat. Biotechnol. *22*, 62–69.

Parsons, A.B., Lopez, A., Givoni, I.E., Williams, D.E., Gray, C.A., Porter, J., Chua, G., Sopko, R., Brost, R.L., Ho, C.-H., et al. (2006). Exploring the mode-of-action of bioactive compounds by chemical-genetic profiling in yeast. Cell *126*, 611–625.

Pu, L., Amoscato, A.A., Bier, M.E., and Lazo, J.S. (2002). Dual G1 and G2 phase inhibition by a novel, selective Cdc25 inhibitor 6-chloro-7-[corrected](2-morpholin-4-ylethylamino)-quinoline-5,8-dione. J. Biol. Chem. *277*, 46877–46885.

Reese, A.J., and Doering, T.L. (2003). Cell wall α-1,3-glucan is required to anchor the Cryptococcus neoformans capsule. Mol. Microbiol. *50*, 1401–1409.

Roemer, T., Xu, D., Singh, S.B., Parish, C.A., Harris, G., Wang, H., Davies, J.E., and Bills, G.F. (2011). Confronting the challenges of natural product-based antifungal discovery. Chem. Biol. *18*, 148–164.

Taipale, M., Jarosz, D.F., and Lindquist, S. (2010). HSP90 at the hub of protein homeostasis: emerging mechanistic insights. Nat. Rev. Mol. Cell Biol. *11*, 515–528.

Vecchiarelli, A., Pericolini, E., Gabrielli, E., Kenno, S., Perito, S., Cenci, E., and Monari, C. (2013). Elucidating the immunological function of the Cryptococcus neoformans capsule. Future Microbiol. *8*, 1107–1116.

Whelan, W.L., and Kwon-Chung, K.J. (1986). Genetic complementation in Cryptococcus neoformans. J. Bacteriol. *166*, 924–929.

WHO (2011). Rapid Advice: diagnosis, prevention and management of cryptococcal disease in HIV-infected adults, adolescents, and children, W.H.O. Library, ed. (Geneva, Switzerland: WHO Press).

Xu, D., Jiang, B., Ketela, T., Lemieux, S., Veillette, K., Martel, N., Davison, J., Sillaots, S., Trosok, S., Bachewich, C., et al. (2007). Genome-wide fitness test and mechanism-of-action studies of inhibitory compounds in Candida albicans. PLoS Pathog. *3*, e92.

Xu, D., Sillaots, S., Davison, J., Hu, W., Jiang, B., Kauffman, S., Martel, N., Ocampo, P., Oh, C., Trosok, S., et al. (2009). Chemical genetic profiling and characterization of small-molecule compounds that affect the biosynthesis of unsaturated fatty acids in Candida albicans. J. Biol. Chem. *284*, 19754–19764.

Zhai, B., Wu, C., Wang, L., Sachs, M.S., and Lin, X. (2012). The antidepressant sertraline provides a promising therapeutic option for neurotropic cryptococcal infections. Antimicrob. Agents Chemother. *56*, 3758–3766.